

(1) $\exists x \text{ and } \exists X \text{ where } ((X)_\perp^0)^\perp = (X)_\Phi = x$

the next defined mapping Φ :

The deformation of the body from the reference configuration \mathcal{U}_0 is characterized by

In a most convenient way among all the configurations that the body can sustain.

Frequently, the reference configuration is fixed for a given study and is chosen arbitrary

p in the two configurations under consideration.

the mappings χ_0 and χ_1 take $p \leftarrow X$ and $p \leftarrow x$, thus X and x are the positions of particle

configuration relative to which the changes are to be measured Δ_0 . Here, see figure 3.1,

two configurations: the configuration that one wishes to analyze U_i , and the reference

stimuli one needs to know the changes in geometrical characteristics between at least

p and position x , $\mathcal{U}_0 = \chi_0(B)$ (see figure 3.1). To describe solid's respond to an external

The configuration of a body is defined as a one-to-one mapping between the particle

space then exposed to some external stimuli like force, pressure or heat.

A particular body can change its configuration and therefore the occupied region in the

is the domain Ω occupied by the body in a given configuration, here also named *geometry*.

The set of all points in space, corresponding to the locations of all the particles, is called the **configuration space**.

material points). Each particle is located at some definite point x in three dimensions (or

of matter. In continuous mechanics, a body B is composed of a set of particles p (or points) which have properties, and the space occupied by them (volume) measure

composition and completeness fills the space it occupies forming the grammatical (atomic) nature

and consciousness; in a microscopic microscope, a soul object is described as homogeneous and continuous "body". i.e. the substance of the object have a infinite

A body is the macroscopic appearance of an object, and is defined by its geometrical and constitutive character.

depends on the application of forces or other external variables; [5]

concerns mechanics is the thermodynamic description of how objects that occur in nature respond to the application of forces or other external stimuli.

continuities mechanics is the mathematical description of how objects that exist in nature

3.2.1 Deformation and strain

Yerba Buena

3.2. Coulombous Mechanics

3.2 Continuous mechanics

3.2 Continuous mechanics

3.1 Introduction
Analyze et justifiez les différentes parties de ce chapitre

Background and state of the art

Therefore, the coordinates of both, the particle and the attached variable, do not change for all $p \in B$. Here the coordinate system remains consistent and moves with the particle.

$$m = M(p)$$

are defined by the function

density, can be defined for each individual particle. In such cases, the body characteristics depending on the choice of independent variables. Some physical characteristics, such as mass

There are two classical techniques used to describe the body physical characteristics de-

Eulerian and Lagrangian formulations

the body and the density $g(x)$ is related to the position of the body particle.
where du is the volume of the material element. Thus, the property $G(U)$ is related to

$$G(U) = \int_{U_0}^{U_1} g(x) du$$

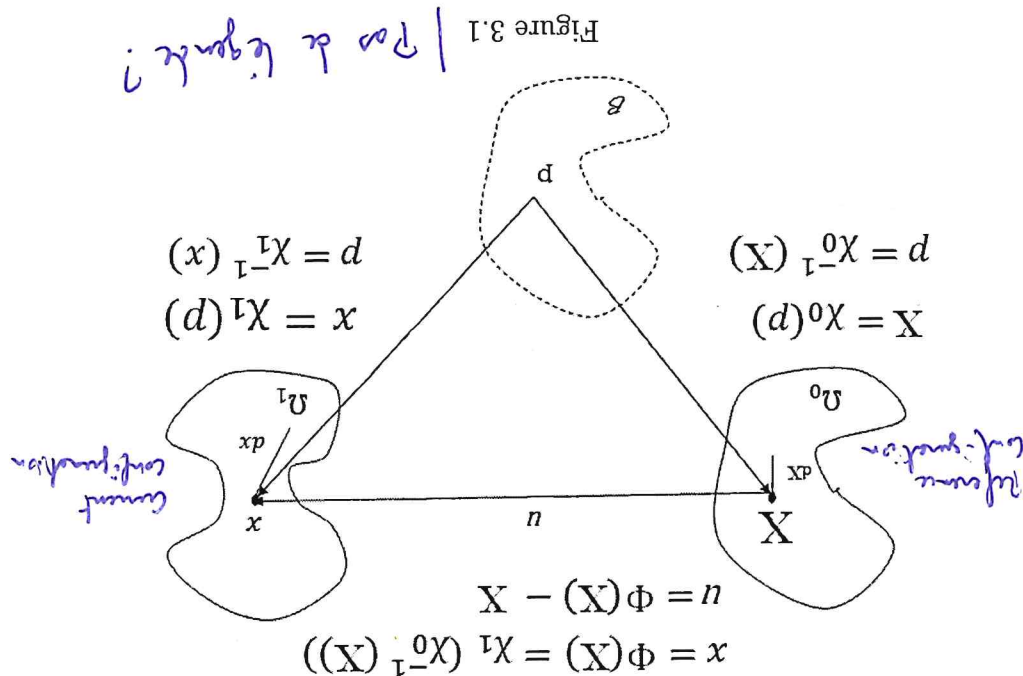
$g(x)$ such that:

the body \mathcal{B} in the current configuration (such as the body mass m). There exists a density suppose that $G(U)$ is the value of some extensive physical property associated with

$$(3.2) \quad u(X) = (X - X_0)\Phi$$

B

The displacement u of a particle is the difference between its position in the analyzed configuration (or current configuration) and its position in the reference configuration.



$$(3.6) \quad \Lambda \int g(x) J d\alpha = \int g(p) p d\alpha$$

The Jacobian determinant of the deformation gradient tensor J is a measure of the volume variation during the deformation. The Jacobian determinant can be used to relate extensive physical properties in the current and reference configurations by the next equality:

$$(3.5) \quad d\alpha = \det(J) J d\alpha$$

In addition to the mapping line elements, the deformation gradient tensor also allows the mapping of differential volumes as:

$$(3.4) \quad dx = F \cdot dX.$$

Considering infinitesimal quantities, the deformation gradient relates the segment dx in the current configuration (Figure 3.1) to the corresponding deformed segment dX in the reference configuration as:

$$(3.3) \quad \frac{X\theta}{\theta} = \frac{X}{(X)\Phi\theta} = F$$

In mathematical formulation the deformation gradient F is the Jacobian matrix of the deformation $\Phi(X)$:

These approaches are distinguished by three important aspects: the mesh description, the stress tensor and momenta equilibrium and the strain measure. The advantages and drawbacks of two formulations will be discussed later in this chapter. Further, only large-angle formulation is used to describe the continuous deformation of soft tissues.

Here the coordinate system is fixed and the particles coordinate are changing. Therefore, the position of particle and any related quantity changes during the deformation. We call a Eulerian or spatial coordinates and their application is called Eulerian or spatial description.

Instead of defining body characteristics as a function of body particles, one can define it directly as a function of particle location in current configuration by using the relation $x = X_i(p)$, and therefore it defines material description.

We call X Lagrangian or material coordinates and their application is called Lagrangian calculations. Since a particle is an abstract entity it cannot be used in numerical calculations, therefore the particle is described by its location in reference configuration along the deformation. In addition, the particle is an abstract entity it cannot be used in numerical calculations, therefore the particle is described by its location in reference configuration along the deformation.

$$\det(C - uI) = -u^3 + I_1(C)u^2 - I_2(C)u + I_3(C) \quad (3.10)$$

The interpretation is that, the body "stretch" consists (locally) of three mutually orthogonal principal stretches, "the principal stretches". The latter are scalar combinations of C components that do not change under coordinate transformations for a given body configuration. The use of invariants will be an essential part of constitutive modeling, because the behavior of a material should not depend on the coordinate system.

$$I_1(C) = \text{tr}C, \quad I_2(C) = \frac{1}{2} [\text{tr}C^2 - (\text{tr}C)^2], \quad I_3(C) = \det(C) \quad (3.9)$$

Where are three particular functions of C called the principal scalar invariants. The Green deformation tensor $C = F^T \cdot F$. U is also called the right stretch tensor. Since there is a one-to-one relation between U and U^2 , for the simplification of numerical calculations the stretch tensor can be replaced by the F .

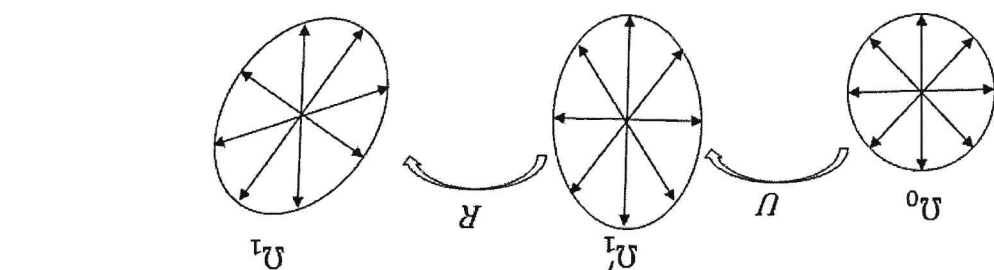
$$F = R \cdot U. \quad (3.8)$$

Using polar decomposition theorem, the deformation tensor can be written as the product of a proper orthogonal tensor R representing the rotational part, and a symmetric positive defined tensor U representing the body distortion.

$$\frac{|Xp|}{|xp|} = \ddagger \quad (3.7)$$

is deformed as the ratio of the deformed line elements to the length of the corresponding undeformed line element:

The deformation gradient tensor represents the entire body deformation, which consists of rigid body rotation and body "stretch" (see Fig. 3.2). As dX and dx are differential segments, the map F is not affected by rigid-body translations. Generally, the body stretch is deformed as the ratio of the deformed line elements to the length of the corresponding undeformed line element:



solving a boundary-value problem, this stress defines the boundary conditions. By external forces through physical contact along the boundary. When formulating and 615

The stress on the boundary $\partial\Omega$ of the region occupied by the studied body is applied

vector and its projection on the tangential axis define the shear stress vector.

vector and its projection on normal axis n defines the normal stress

$d\sigma(n)$ orientation. The stress vector projection on normal axis n depends on the

Therefore $t_n(x)$ varies from point to point in intensity and orientation depending on the

traction vector $t_n(x)$ is defined as contact force per unit area da in the limit as $da \rightarrow 0$.

internal surface enclosing a volume element (Fig. 3.3). In general terms, the stress (or the

contact forces can act on the external surface of the body or on a imaginary

$$\tau = \frac{d\sigma}{dn} = \tau_b. \quad (3.14)$$

following relation:

(Lagrangean coordinates) and body forces per unit deformed volume $b(x)$ is given by the

the body surface). The relation between body forces per unit undeformed volume $b(X)$

are categorized in body forces (acting at the distance) and contact forces (acting on

force is a force exchanged by the particle in the system. The external forces, in turn,

a force caused by an external agent outside of the system, and contrariwise an internal

Generally, forces are categorized as internal and external forces. An external force is

Body and contact forces

*as the boundary shown
if we put now m = 0 on*

The Green-Lagrange tensor is commonly used in practice as it can be computed without prior knowledge of the eigenvectors of Green deformation tensor C . *if a function which measure?*

$$E = \frac{1}{2}(U^2 - I) = \frac{1}{2}(C - I) \quad (3.13)$$

Then $m = 2$ the function is named the Green-Lagrange strain tensor:

$$f(x) = \frac{m}{1}(x_m - 1) \quad (m \neq 0) \quad \text{and} \quad f(x) = 0 \quad \begin{cases} \text{if } m = 0 \\ \text{if } m < 0 \end{cases} \quad (3.12)$$

In orthogonal coordinate system an admissible function is:

one-to-one manner, and what completely vanishes in the reference configuration.

a measure of strain can be any monotonically increasing function related to stretch in a therefore, the previously defined strain is no more applicable. For large deformations, *in this case* therefore, the one is modeling biological soft tissues, large deformations have to be considered.

Then one is modeling biological soft tissues, large deformation have to be considered.

stretch tensor U is equal to identity tensor I . The strain in such case is equal to zero.

Then the body is not deformed, the deformation gradient F and therefore the right

$$\epsilon = \frac{Xp}{xp - x} \quad (3.11)$$

undeformed line element:

of the change in length of the deformed line element to the length of the corresponding referring to small deformations, the engineering nominal strain is defined as the ratio

Strain measures

- $T_N = P \cdot N$, P is called first Piola-Kirchhoff stress tensor,

Accordingly, two pseudostress tensors are defined based on pseudostress vectors:

- the contact force $d\mathbf{f}$ per unit area in reference configuration \mathcal{A} .
 - the contact pseudoforce $d\mathbf{f}_p$ per unit area in reference configuration $d\mathcal{A}$.

Next, two pseudostress vectors are defined (Fig. 3.4):

have to be converted in to true stress for any interpretations.

The definition of any measure with respect to the deformed configuration is less practical as the current configuration is usually unknown a priori. For the simplification of mathematical formulation, a new pseudostress is defined in the Lagrangian coordinate space named engineering stress. The engineering stress have no physical meaning and

stress tensor.

When large deformations are considered, the reference and current configurations of the body are significantly different and a clear distinction has to be made between them. The traction vector τ_n is defined in Eulerian coordinates (body current configuration) and is also called the true stress. Accordingly, the Cauchy stress tensor σ is called the true stress.

(3.16) $t_n = o \cdot n$ where $t_i = o_{i,j} n_j$

Cauchy's law states that there exists a Cauchy stress tensor σ which maps linearly the normal to a surface to the stress vector acting on that surface, according to the next

Cauchy's Law

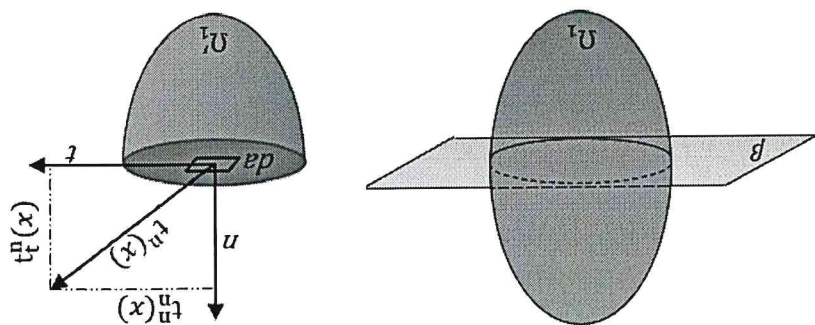
$$(x)_{u\tau} = (x)_{u-\tau}$$

$$(x)_{u\bar{t}} = (x)_{u\bar{t}} -$$

and opposite.

Cauchy's lemma states that traction vectors acting on opposite sides of a surface are equal across a boundary.

Figure 3.3: True stress vector $\tau_n(x)$ at point x on the haptic surface created by the cutting plane θ of normal n passing through the point x .



$$(3.19) \quad \int_{U_0}^{U_1} (p_1 f - p_0) du = 0 \quad \text{and} \quad p_1 f = p_0$$

Using the relation 3.6 one can deduce that:

$$\int_{U_0}^{U_1} p_1 du = \int_{U_0}^{U_1} p_0 dV = \text{const.}$$

current configuration p .

between the body density in the reference configuration p_1 and the body density in the possible body configurations. For a Lagrangian formulation, this results in a relation $\frac{d}{dt} m(U) = 0$ requires that the body mass remains constant throughout all

$$(3.18) \quad m(U) = \int_U p(X) dV$$

The mass m of a body with the density p , that initially the space region U_1 is given by:

Conservation of mass

645 three conservation laws must to be satisfied by physical system subject to any applied boundary conditions: conservation of mass, conservation of linear momentum and conservation of angular momentum. The resulting equations describe partially the mechanical behavior of a continuous body.

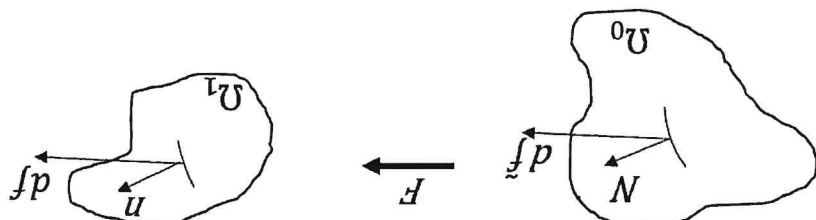
3.2.3 Conservation equations

$$(3.17) \quad \sigma = f^{-1} F \cdot P = f^{-1} F \cdot S \cdot F^T$$

The three stress tensors are linked by the next relation

$$640 \quad \bullet \quad T_N = S \cdot N, \quad S \text{ is called second Piola-Kirchhoff stress tensor.}$$

Figure 3.4: Deformation of area dA into area $d\bar{a}$. The force dF acting on deformed area $d\bar{a}$ and the pseudoforce $d\bar{f}$ acting on undeformed area dA



define a universal material behavior capable to model the material response to all possible strain of a physical system under the action of a external stimuli. It is very complex to define a constitutive models, called also material models, define the relation between stress and

3.2.4 Constitutive models

With the traction on the surface related to the stress through $T_n = S \cdot N$. For the simplified traction of mathematical calculus, the constitutive equations are formulated in terms of the second Piola-Kirchhoff stress tensor using the relations 3.17.

$$P^1_j = p_0, \quad \Delta^0 \cdot S \cdot F_T + P^0 q = 0, \quad S = S_T \quad (3.24)$$

In summary, the conservation equations are fulfilled if and only if the following local conditions are fulfilled at each point in the body:

$$S = S_T \quad (3.23)$$

The relation 3.22 demands that the second Piola-Kirchhoff stress tensor by a symmetric tensor:

$$\int_{\Omega_0} X \times P^0 b(X) dV + \int_{\partial\Omega_0} X \times T_N(X) dA = 0 \quad (3.22)$$

The conservation of angular momentum requires that the resultant momentum on any part of the body about a fixed point O equals the rate of increasing of its angular momentum (about O). For a static problem, the integral form of the conservation of angular momentum is defined as:

Conservation of angular momentum

Here the P^i_j are the components of first Piola-Kirchhoff stress tensor. The equilibrium equation can be formulated in terms of the second Piola-Kirchhoff stress tensor by using 3.17 relations.

The conservation of the linear momentum requires that the total forces acting on the body to be equal to the time rate change of the linear momentum is neglected and thus the next equilibrium is obtained:

$$P^0 b + \Delta^0 \cdot P = 0 \quad (3.21)$$

The conservation of the linear momentum requires that the total force acting on the deformed solid. The total force acting on the body \mathcal{B} is defined as:

Assume that a body \mathcal{B} defined on a arbitrary region Ω_1 , with boundary T_1 , is subjected to a body-force p_b and the surface traction a_T . And let X be the particle location in the

CHAPTER 3. BACKGROUND AND STATE OF THE ART

$$K = \frac{E}{(1-\nu)} \text{ and } \nu = \frac{2(1-\nu)}{E}$$

Young's modulus and Poisson ratio by the next relations:

the ratio between longitudinal strain to the transverse strain describes the body shape change. For small deformations the bulk modulus and shear modulus are linked to the shear modulus as the ratio of shear stress to the shear strain; and the Poisson ratio as the shear modulus as measure of a material's resistance to compression,

700

$$I_1 = \frac{I_1}{I_3}; I_2 = \frac{I_2}{I_3} - , \text{ etc. } b_i = ?$$

! all right

atropic strain invariants:

For the simplification of potential expressions we define the first and the second devi-

695

functions for characterization of biological soft materials. *Hydrogel*

tensor C previously defined in equation 3.9. Next, we introduce the most used potential can by written as a function of principal invariants (I_1, I_2, I_3) of the Green deformation

Moreover, if the material is isotropic, the stored strain energy W of a hyperelastic material

$$S = \frac{\partial W(E)}{\partial E} = 2 \frac{\partial \phi(C)}{\partial C}$$

where the coefficient of proportionality λ is named Young's modulus.

$$\sigma = \lambda e,$$

the Hook's law

Considering small deformations, the stress-strain law of a linear material is given by

690

a external force is removed. In this case the strains are said to be reversible.

property of a solid material to return to its original size and shape when the influence of biological soft tissues are modeled using elastic materials model. The elasticity is the

material is independent (dependent) of the position within the body.

685

Homogeneous or heterogeneous materials: the response of a homogeneous (heterogeneous)

J is equal to 1.

For a incompressible material the Jacobian determinant of the deformation tensor the volume is change (unchanged) during the deformation and the density remains constant. Thus, for a incompressible material the response of a homogeneous (heterogeneous)

680

an applied load is independent (dependent) of the direction of loading.

675

Isotropic or anisotropic materials: the response of a isotropic (anisotropic) material to

Based on different characteristics biological materials are classified into:

can be

conditions. Thus, for one material, several constitutive models can be defined depending

a given model

725

We consider a body Ω^0 , which occupies in the reference configuration the domain Ω^0 with a boundary I^0 . The governing equations for the mechanical behavior of a continuous body

720 are:

1. Conservation of mass $p_1 f = p_0$
2. Conservation of linear momentum $\nabla \cdot P + \rho b = 0$
3. Conservation of angular momentum $F \cdot P = P_T \cdot F_T$
4. Constitutive equations

$$5. \text{ Measure of strain } E = \frac{1}{2}(C - I)$$

$$6. \text{ Boundary condition: } e_i \cdot N \cdot P = e_i \cdot t \text{ on } I^0_i$$

$$7. \text{ Internal continuity condition: } [e_i \cdot N \cdot P] = 0 \text{ on } I_{int}^0$$

Governing equations of Lagrangian formulation

bulk modulus respectively. And J_m is the limiting value of $(I_1 - 3)$

Where, as previous the u and K constants are the initial shear modulus and the initial bulk modulus respectively. And J_m is the limiting value of $(I_1 - 3)$

$$W = -\frac{1}{2}J_m \ln \left(1 - \frac{J_1}{I_1 - 3} \right) + K \left(\frac{J_2}{J_2 - 1} - \ln J \right) \quad (3.27)$$

The potential function of a Gent material model is defined as:

Gent potential function

Where the constants u_1 and u_2 describing the material properties are linked to the initial shear modulus $P = (u_1 + u_2)$. And the constant K is the initial bulk modulus.

$$W = \frac{u_1}{2}(I_1 - 3) + \frac{u_2}{2}(I_2 - 3) + \frac{K}{2}(J - 2)^2 \quad (3.26)$$

The potential function of a Mooney-Rivlin material is defined as:

Mooney-Rivlin potential function

Where u and K are initial shear modulus and initial bulk modulus respectively.

$$W = \frac{u}{2}(I_1 - 3) + \frac{K}{2}(J - 1)^2 \quad (3.25)$$

function is based only on the first invariant and is given by

The Neo-Hookean law is an extension of the Hook's law to large deformations. The potential

function is based only on the first invariant and is given by

Neo-Hookean potential function

where $3 \log_e \frac{J}{J_0}$ is the potential and J_0 is the initial volume.

where $3 \log_e \frac{J}{J_0}$ is the potential and J_0 is the initial volume.

where $3 \log_e \frac{J}{J_0}$ is the potential and J_0 is the initial volume.

CHAPTER 3. BACKGROUND AND STATE OF THE ART

705

710

715

720

725

to fluid like materials and a Lagrangian mesh for solid like materials.

In conclusion, an Eulerian mesh usually used to solve problems linked or failure is a important factor in nonlinear analysis with Lagrangian formulation. The limited distortion that most elements can sustain without performance degradation or failure, the magnitude of deformation is limited because of element distortion. Therefore, the nodes are coincident with the material points, the elements deform with main. As the nodes are coincident with the material points, the large deformation does not affect mainly the large deformation do. An important drawback of a Lagrangian mesh affects mainly the large deformation due to the boundary and interface conditions in multi-dimensional problems. This implies important complications in multi-dimensional problems.

nodes. The boundary and interface conditions have to be defined on point which are not mesh the boundary and interface nodes. On the other hand, in a Eulerian formulation, the boundaries and material interfaces throughout the entire deformation. Thus, the boundary conditions are defined directly on the respective nodes. In a Eulerian formulation, the boundaries and material boundaries remain coincident with body elements (see Figure 3.5.a).

In a Lagrangian mesh, the boundary and interface nodes remains coincident with body trajectory corresponds with material points trajectory and no material passes between in a Lagrangian mesh, the Lagrangian coordinates of nodes are time invariant, nodal throughout the deformation, the material points will belong to different elements. Whereas, case the mesh has to be large enough to contain the body in its current configuration with spatial points) and the material point change in time (see Figure 3.5.b). In this formulation, the Eulerian mesh, the Eulerian coordinates of nodes are fixed (coincident throughout the deformation).

The mesh description depends on the chosen independent variables (Eulerian or Lagrangian domain Ω_0 into many small control volumes Ω_i . problem are associated with a computational mesh which represents a subdivision of the function values at a finite number of discrete locations. The unknowns of the discrete partial derivatives are discretized, so as to obtain a set of algebraic equations for the compute such approximations. The computational domain, the unknown solution, and end, the finite element (FE) method has become the standard numerical calculation to cannot be solved analytically, therefore approximate methods are developed. To this terms of partial differential equations (PDE). For the majority of problems, the PDEs are previously described, in continuous mechanics the body deformation is expressed in traction continuity condition together with the traction boundary condition and interior tractions of generalized Moementum Balance (GMB).

3.3 Finite Element Discretization

As previously described, in continuous mechanics the body deformation is expressed in traction continuity condition together with the traction boundary condition and interior tractions of generalized Moementum Balance (GMB).

Where we note T^i_t , the set of prescribed traction t on the body boundary F^0 ; and I_{int}^0 is the union of all surfaces where the stresses are discontinuous in the body (material interfaces). Where we note T^i_t , the set of prescribed traction t on the body boundary F^0 ; and I_{int}^0 is the union of all surfaces where the stresses are discontinuous in the body (material interfaces).

The momentum equations and the traction boundary conditions, usually called the strong form of GMB cannot be directly discretized by FE method. The strong formulation of this problem imposes the C_i continuity conditions on the field variables. Therefore, the GBN equations impose the C_i continuity conditions on the field variables. Therefore, weak domains with different material interfaces. In order to overcome these difficulties, complex domains with always exist. This is true especially in the case of the solution of this problem does not always exist. This is due to numerical difficulties of the redaction in the use of easy-to-construct and implement polynomials.

Because of the redaction in the use of function smoothness, the weak forms never give an exact solution but one can obtain a relatively accurate solution with the discrētization refinement.

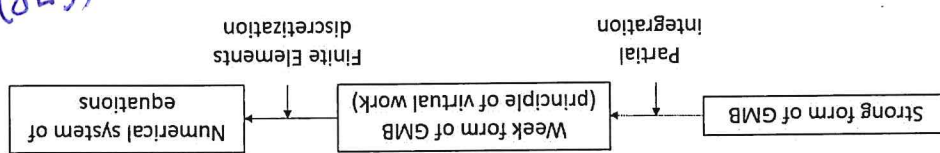
780 The weak formulation of GMB reduces the continuity requirements thereby allowing the use of easy-to-construct and implement polynomials.

775 Weak formulations are preferred. The weak formulation of GMB reduces the continuity requirements thereby allowing the use of easy-to-construct and implement polynomials.

770 The GBN equations impose the C_i continuity conditions on the field variables. Therefore, the GBN equations impose the C_i continuity conditions on the field variables. Therefore,

(Gn3)

765 The strong form of GMB cannot be discretized by FE method. The strong formulation of this problem imposes the C_i continuity conditions on the field variables. Therefore,



760 First the momentum equations with given boundary conditions is multiplied by a suitable test functions. The test function has to satisfy all displacement boundary conditions and to be smooth enough so that all derivatives in momentum equations are well defined. Then performing an integration by parts, the weak formulation of GMB is obtained, also called the principle of virtual work. cite Beleytschko

755 3.6. First the momentum equations with given boundary conditions is multiplied by a suitable test functions. The test function has to satisfy all displacement boundary

750 conditions and to be smooth enough so that all derivatives in momentum equations are well defined. Then performing an integration by parts, the weak formulation of GMB is obtained, also called the principle of virtual work. cite Beleytschko

745 3.6. First the momentum equations with given boundary conditions is multiplied by a suitable test functions. The test function has to satisfy all displacement boundary

740 conditions and to be smooth enough so that all derivatives in momentum equations are well defined. Then performing an integration by parts, the weak formulation of GMB is obtained, also called the principle of virtual work. cite Beleytschko

735 3.6. First the momentum equations with given boundary conditions is multiplied by a suitable test functions. The test function has to satisfy all displacement boundary

730 conditions and to be smooth enough so that all derivatives in momentum equations are well defined. Then performing an integration by parts, the weak formulation of GMB is obtained, also called the principle of virtual work. cite Beleytschko

725 subsection:lagrangian meshes

720 subsection:lagrangian meshes

715 subsection:lagrangian meshes

710 subsection:lagrangian meshes

705 subsection:lagrangian meshes

700 subsection:lagrangian meshes

695 subsection:lagrangian meshes

690 subsection:lagrangian meshes

685 subsection:lagrangian meshes

680 subsection:lagrangian meshes

675 subsection:lagrangian meshes

670 subsection:lagrangian meshes

665 subsection:lagrangian meshes

660 subsection:lagrangian meshes

655 subsection:lagrangian meshes

650 subsection:lagrangian meshes

645 subsection:lagrangian meshes

640 subsection:lagrangian meshes

635 subsection:lagrangian meshes

630 subsection:lagrangian meshes

625 subsection:lagrangian meshes

620 subsection:lagrangian meshes

615 subsection:lagrangian meshes

610 subsection:lagrangian meshes

605 subsection:lagrangian meshes

600 subsection:lagrangian meshes

595 subsection:lagrangian meshes

590 subsection:lagrangian meshes

585 subsection:lagrangian meshes

580 subsection:lagrangian meshes

575 subsection:lagrangian meshes

570 subsection:lagrangian meshes

565 subsection:lagrangian meshes

560 subsection:lagrangian meshes

555 subsection:lagrangian meshes

550 subsection:lagrangian meshes

545 subsection:lagrangian meshes

540 subsection:lagrangian meshes

535 subsection:lagrangian meshes

530 subsection:lagrangian meshes

525 subsection:lagrangian meshes

520 subsection:lagrangian meshes

515 subsection:lagrangian meshes

510 subsection:lagrangian meshes

505 subsection:lagrangian meshes

500 subsection:lagrangian meshes

495 subsection:lagrangian meshes

490 subsection:lagrangian meshes

485 subsection:lagrangian meshes

480 subsection:lagrangian meshes

475 subsection:lagrangian meshes

470 subsection:lagrangian meshes

465 subsection:lagrangian meshes

460 subsection:lagrangian meshes

455 subsection:lagrangian meshes

450 subsection:lagrangian meshes

445 subsection:lagrangian meshes

440 subsection:lagrangian meshes

435 subsection:lagrangian meshes

430 subsection:lagrangian meshes

425 subsection:lagrangian meshes

420 subsection:lagrangian meshes

415 subsection:lagrangian meshes

410 subsection:lagrangian meshes

405 subsection:lagrangian meshes

400 subsection:lagrangian meshes

395 subsection:lagrangian meshes

390 subsection:lagrangian meshes

385 subsection:lagrangian meshes

380 subsection:lagrangian meshes

375 subsection:lagrangian meshes

370 subsection:lagrangian meshes

365 subsection:lagrangian meshes

360 subsection:lagrangian meshes

355 subsection:lagrangian meshes

350 subsection:lagrangian meshes

345 subsection:lagrangian meshes

340 subsection:lagrangian meshes

335 subsection:lagrangian meshes

330 subsection:lagrangian meshes

325 subsection:lagrangian meshes

320 subsection:lagrangian meshes

315 subsection:lagrangian meshes

310 subsection:lagrangian meshes

305 subsection:lagrangian meshes

300 subsection:lagrangian meshes

295 subsection:lagrangian meshes

290 subsection:lagrangian meshes

285 subsection:lagrangian meshes

280 subsection:lagrangian meshes

275 subsection:lagrangian meshes

270 subsection:lagrangian meshes

265 subsection:lagrangian meshes

260 subsection:lagrangian meshes

255 subsection:lagrangian meshes

250 subsection:lagrangian meshes

245 subsection:lagrangian meshes

240 subsection:lagrangian meshes

235 subsection:lagrangian meshes

230 subsection:lagrangian meshes

225 subsection:lagrangian meshes

220 subsection:lagrangian meshes

215 subsection:lagrangian meshes

210 subsection:lagrangian meshes

205 subsection:lagrangian meshes

200 subsection:lagrangian meshes

195 subsection:lagrangian meshes

190 subsection:lagrangian meshes

185 subsection:lagrangian meshes

180 subsection:lagrangian meshes

175 subsection:lagrangian meshes

170 subsection:lagrangian meshes

165 subsection:lagrangian meshes

160 subsection:lagrangian meshes

155 subsection:lagrangian meshes

150 subsection:lagrangian meshes

145 subsection:lagrangian meshes

140 subsection:lagrangian meshes

135 subsection:lagrangian meshes

130 subsection:lagrangian meshes

125 subsection:lagrangian meshes

120 subsection:lagrangian meshes

115 subsection:lagrangian meshes

110 subsection:lagrangian meshes

105 subsection:lagrangian meshes

100 subsection:lagrangian meshes

95 subsection:lagrangian meshes

90 subsection:lagrangian meshes

85 subsection:lagrangian meshes

80 subsection:lagrangian meshes

75 subsection:lagrangian meshes

70 subsection:lagrangian meshes

65 subsection:lagrangian meshes

60 subsection:lagrangian meshes

55 subsection:lagrangian meshes

50 subsection:lagrangian meshes

45 subsection:lagrangian meshes

40 subsection:lagrangian meshes

35 subsection:lagrangian meshes

30 subsection:lagrangian meshes

25 subsection:lagrangian meshes

20 subsection:lagrangian meshes

15 subsection:lagrangian meshes

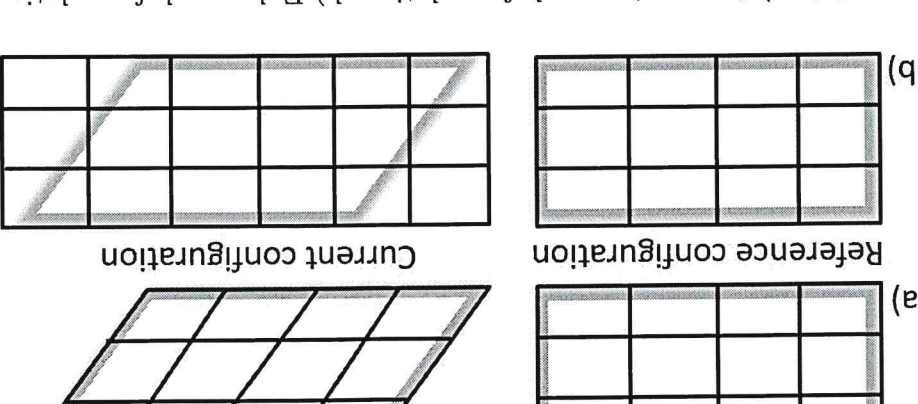
10 subsection:lagrangian meshes

5 subsection:lagrangian meshes

0 subsection:lagrangian meshes

3.3.2 Lagrangian mesh

Figure 3.5: a) Lagrangian mesh formulation. b) Eulerian mesh formulation



The element's shape aspect ratio is computed using only the corner nodes of the element (Figure 3.8). First, two lines are created: one through a node (K) and the midpoint of the opposite edge (K'), the second through the midpoint of the other two edges (J) and the midpoint of previously defined lines. Then two rectangles are created, each rectangle having a pair of edges parallel to one another (I). The aspect ratio of a rectangle is defined as the ratio between the longer side's edges midpoints. This construction is repeated for each triangle's node resulting in 6 rectangles.

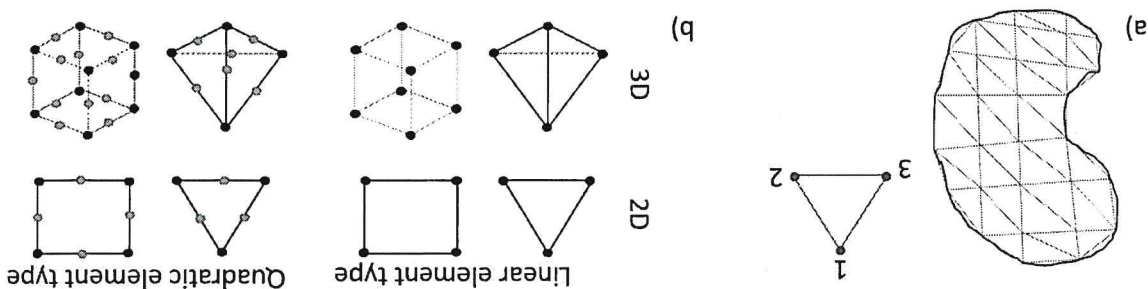
805

Triangle aspect ratio

In the following only shape parameters of linear triangular elements are presented. 800

As in a Lagrangian mesh the nodes are following the motions, for large deformations finite elements can be highly distorted. Therefore, the shape quality is generally followed by all types. In this way, the problem of finding the displacement of every point within the element is replaced by the problem of finding the displacement of a finite number of points. The displacement within an element is fixed by the values of the nodes of each point within the element. In this way, the problem of finding the displacement of every point within the element is solved by the values of the nodes of each point within the element for a quadratic type (Figure 3.7.b). The displacement corners and mid-sides of the elements for a quadratic type, and at the element nodes. The nodes are at the corners of the elements for a linear type, and at the element nodes. The mechanical displacement is approximated at the discretization points called finite 795

Figure 3.7: a) Discretization of a 2D domain with triangular finite elements: Lagrangian mesh. b) Different types of finite elements



From the weak form of the GFM equations, the numerical system of equations is formulated by using finite elements interpolants for the mechanical displacement and the test functions. The whole domain is discretized into a number of smaller areas or volumes which are called finite elements and their assembly is called a mesh. Elements can be of various shapes (as shown in Figure 3.7a), quadrilateral or triangular in two dimensions, and tetrahedral or hexahedral in three-dimensions. 785

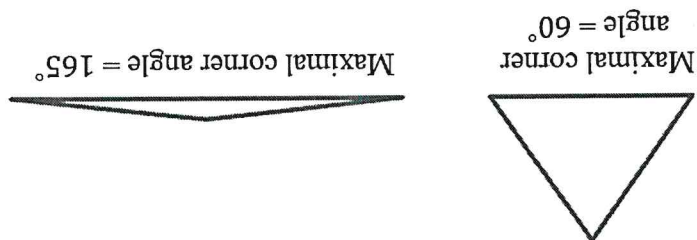
795

The skewness of a triangular element is computed using the equivalent volume deviation method. It is defined as the difference between the optimal and real cell size over the

Skewness

as the worst value over the triangles defined by the tetrahedra's faces and cross-sections. The aspect ratio and the maximal corner deviation of a tetrahedra is computed using the definition of the same measure on a triangle. The elements shape parameter is assigned

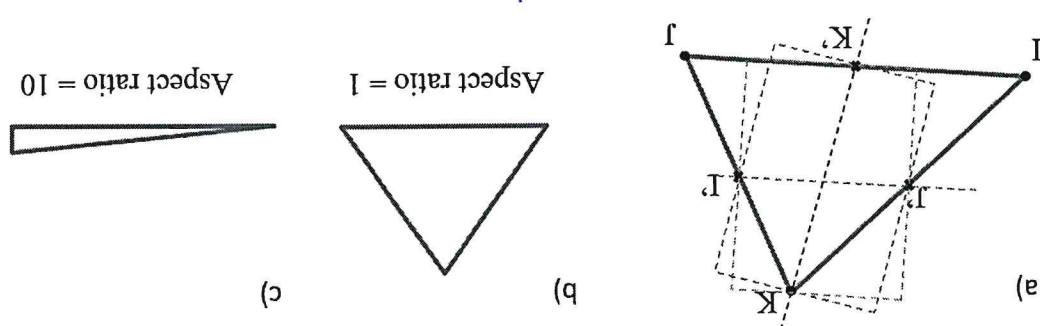
Figure 3.9: Example of triangles with different maximal corner angles.



possible maximum corner angle is 60°. An element having a maximal corner angle larger than 165° is considered as bad shape element, large corner angles may degrade the solution performance. Figure 3.9 shows a triangle with a good (60°) and bad (165°) quality.

Triangle maximum corner angle

Figure 3.8: Computation of aspect ratio for a triangle



The best possible aspect ratio is 1 and is represented by an equilateral triangle. An element with an aspect ratio larger than 20 is considered as bad aspect element, large aspect ratio may degrade solution performance. The aspect ratio is divided by squared root of 3. over the 6 rectangles divided by squared root of 3.

For the following, we identify T_A as the target surface and T_B as the contact surface (Figure 3.11).

- if the surface T_A is larger than T_B , the surface T_A denotes the target and the T_B the contact surfaces.
- if T_A is a concave surface getting in contact with the convex surface T_B , the surface T_A defines the target and T_B the contact surface.
- if the one body A is stiffer than the body B , the surfaces T_A defines the target and T_B the contact surfaces.

The choice of the surfaces is made following the next guidelines:

$$T = T_A \cup T_B.$$

two bodies:

intersection of two bodies. The contact interface is the intersection of the surfaces of the with boundaries T_A and T_B respectively (see Figure 3.11). Also, we note \mathcal{D} the domain of

Let's consider two different bodies A and B and their occupied domains \mathcal{D}_A and \mathcal{D}_B . Surface contact method is used to solve the multi-body interaction problems. deformation and the bodies will pass through each other. Here, an asymmetric surface-to-surface contact and two bodies are separated with no common nodes, no interaction will occur during the If two bodies are connected together, the nodes have to be connected together.

830

840

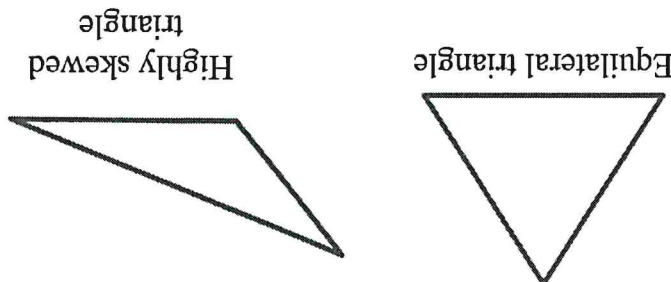
855

860

Handwritten notes:
Is it possible to define a contact surface for a curved boundary?
Is it possible to define a contact surface for a curved boundary?
Is it possible to define a contact surface for a curved boundary?

3.4 Contact mechanics

Figure 3.10: Example of triangles with different skewness.



optimal cell size. The optimal size is the size of an equilateral cell with the same circumradius. According to its definition, the value of 0 indicates an ideal cell, from 0 to 0.75 the cell is considered to have a good quality, from 0.75 to 1 the cell is considered to have a bad quality and a value of 1 indicates a completely degenerated cell (Figure 3.10).

825

$$\mathcal{J}_A \cup \mathcal{J}_B = 0 \quad (3.30)$$

⁸⁵⁵ The bodies implied in a multi-body problem must fulfill the inter-penetrability condition:

Inter-penetrability condition

$$t_A^A + t_B^B = 0, \quad t_A^B + t_B^A = 0 \quad (3.29)$$

Therefore the momentum balance requires:

$$t_A^A = t_A - t_A n_A, \quad t_B^B = t_B - t_B n_B$$

$$t_A^B = t_A \cdot n_A, \quad t_B^A = t_B \cdot n_B$$

tangential components:

On the contact boundary surface Γ the traction vectors \mathbf{T} is decomposed into its normal and

$$t_A + t_B = 0 \quad (3.28)$$

⁸⁵⁰ Traction conditions must follow the balance of momentum across the contact interface:

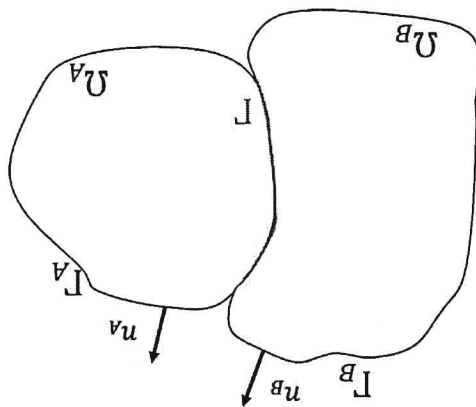
Traction conditions

⁸⁴⁵ In multi-body interaction processes, in addition to standard governing equations, two more contact conditions have to be fulfilled: the two bodies cannot interpenetrate and the traction must satisfy momentum conservation on the contact interfaces.

⁸⁴⁵ Contact conditions must follow the balance of momentum across the contact interface and the two bodies cannot interpenetrate and the traction must satisfy momentum conservation on the contact interfaces.

3.4.1 Contact interface equations

Figure 3.11: Multi-body contact problem.



Where u_f is the material property named **friction coefficient**, Δu_f is the slip increment in the tangential direction and $k(x)$ is a variable computed from the momentum equation. The condition 3.32 is known as sticking condition: the tangential traction is less than zero.

$$\text{if } \|t_t(x)\| = -u_{f_n}(x), \Delta u_t = -k(x)t_t(x), k(x) < 0 \quad (3.33)$$

$$\text{if } \|t_t(x)\| < -u_{f_n}(x), \Delta u_t = 0 \quad (3.32)$$

that bodies A and B which are in contact within the surface L , then for all $x \in L$:
body the Coulomb friction model is applied at each point of the contact interface. Consider the frictional contact behavior is defined using Coulomb friction law. For a continuous

Table 3.1: Surface interaction models and behaviors

Name	body motion in normal direction	body motion in tangential direction	Frictional
Bonded	No	No	Yes, if $f_{sliding} > f_{friction}$
Rough	Yes	No, $f_{friction} \ll f_{sliding}$	Yes, $f_{friction} = 0$
No-separation	No	Yes, $f_{friction} = 0$	Yes, $f_{friction} = 0$
FriCTIONLESS	Yes	Yes	Yes, $f_{friction} = 0$
BONDED	Yes	Yes	Yes, if $f_{sliding} > f_{friction}$

a pure bonded contact, the two bodies are considered as a unique solid body. Contact, the respective components of traction are equal ($t_A = t_B$), which means that, for the body motion is not allowed in normal or tangential direction, once the bodies get in no-separation, frictional and friCTIONLESS. Table 3.1 resume each mechanical behavior. If normal directions, five types of surface interaction models are distinguished: bonded, rough, balancing the involved forces. According to allowed relative body motion in tangential or

The problem in determining whether relative motion will or will not occur is one of tangential force which causes the sliding motion between the two bodies.

body motion along the interface is called **sliding**. The **sliding force**, $f_{sliding}$ is the applied friction force opposing it, the bodies may or may not move relative to the other. The friction force is created. Depending on whether the applied force can overcome the to the applied force is created. Depending on whether the applied force can overcome another tangential force, a **friction force**, $f_{friction}$ tangential to the interface and opposite to the gap between the two bodies.

3.4.2 Surface interaction models

Where g is the gap between the two bodies.

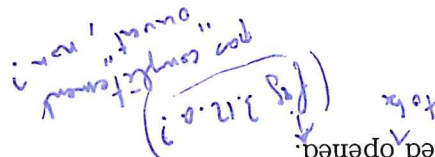
$$t_n \leq 0, u_n - g \leq 0, t_n(u_n - g) = 0 \quad (3.31)$$

specitively, the inter-penetrability condition can be written as:
Decomposing the displacement u into normal and tangential components u_n and u_t re-

Let's consider a point x_B belonging to the body surface T^B and x_A the intersection point of the surface normal n_B with the surface T^A (Figure 3.13). The point to surface distance

Distance measures

006



contact is considered open.

distance is smaller than the pinball radius, the contact is considered closed. Otherwise the distance is over the contact surface points and search for the target surface. If the node to surface side is closed or opened. The status is defined using a sliding pinball (Figure 3.12). The pinball process. Therefore, during the body deformation, the program calculates if the contact is To formulate analytic equations, one has to know exactly the nodes involved in the contact. Therefore, it is very difficult to know a priori where the surfaces will come in contact. The region of contact depends on materials properties and imposed boundary conditions; therefore, it is very difficult to know a priori where the surfaces will come in contact.

895

which will get in contact with each other during the deformation process.

Contact problem presents two primary difficulties. First is the traction conditions computed when frictional models are considered. And second is the unpredictability of regions

009

3.4.3 Contact formulation algorithm: Pure Penalty model

bodies.

Several contact models can be combined to model a physical contact between two bodies.

Therefore, sticking condition is always fulfilled.

completely: $u_A = u_B = 0$. When rough contact is modeled, the friction coefficient μ_f is equal to infinity.

Then a frictionless contact model is used, $u_f = 0$, the tangential tractions vanish

condition.

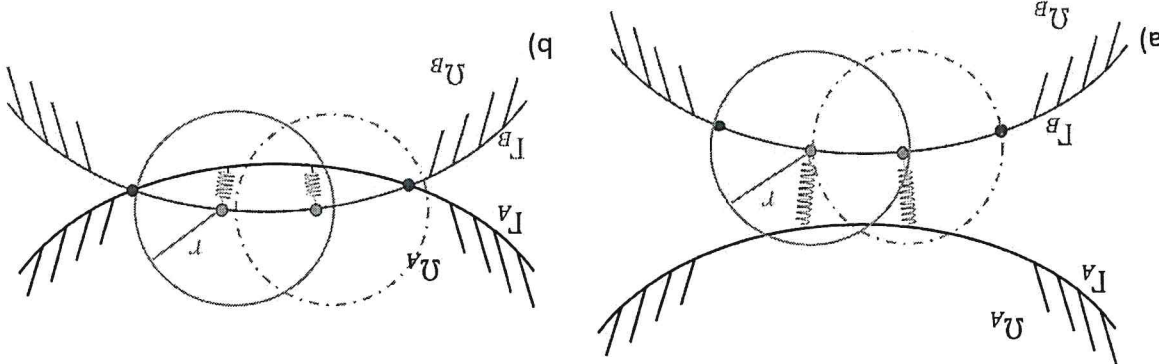
In parallel

885

008

than the critical value, thus no sliding occurs. Reciprocally, condition 3.33 is called sliding condition.

Figure 3.12: Contact status update using a pinball of radius r .



The interested reader is referred to ANSYS contact technology guide for more details on the contact modeling. (Down to nowhere?)

This will be the case in the simulation you will do in this material.

Computing the gap or penetration at single points increases numerical instabilities. Therefore, in this work, the gap and penetration areas computed in an averaged manner over the intersection of the target surface (a) with the projected contact surface (b). Figure 3.14 shows the projected surface areas (c) obtained by averaging the gap and penetration areas (d) over the intersection of the target surface (a) with the projected contact surface (b).

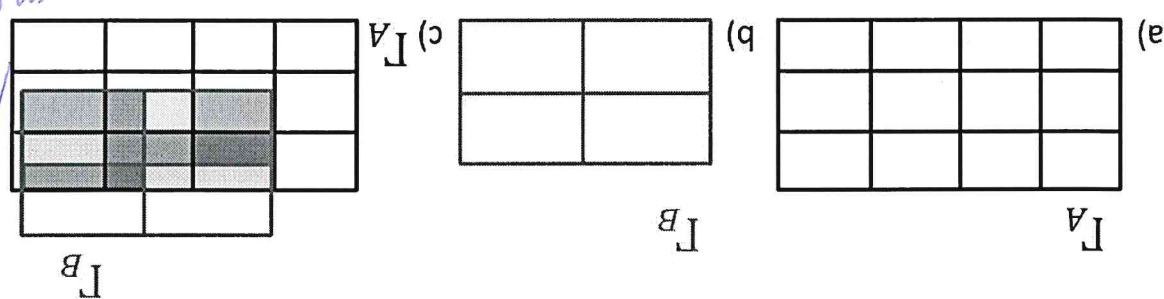
If the intersection point x_A is located inside the pinball area, the node to surface distance

905

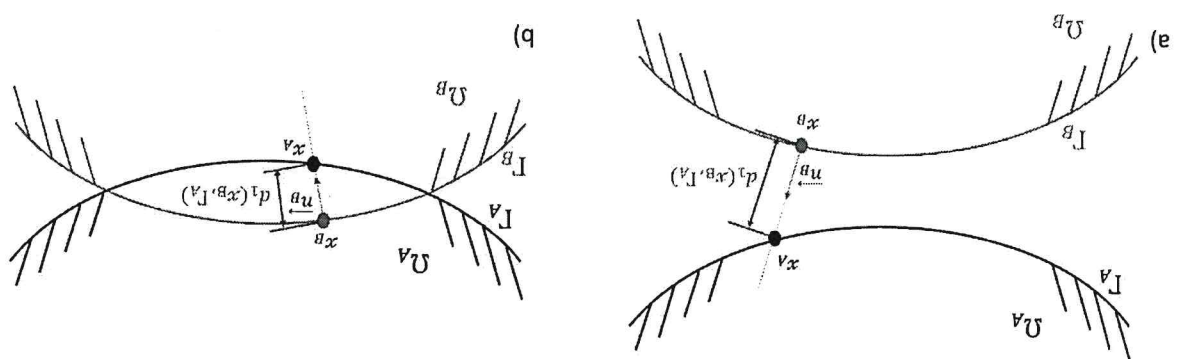
$$d_1(x_B, A) = \|x_B - x_A\| = \left[\sum_{i=1,2,3} (x_i^B - x_i^A)^2 \right]^{\frac{1}{2}} \quad (3.34)$$

$d_1(x_B, A)$ is defined as:

Figure 3.14: The contact surface projection over the target surface: a) Target discretized area; b) Contact discretized area; c) Intersection of the projected surfaces.



The $d_1(x_B, A)$ measure gives the penetration at point x_B . Figure 3.13: a) Body A and body B are close but not in contact. The $d_1(x_B, A)$ measure defines the gap between the bodies at point x_B . b) Body B have penetrated the body A.



depend on the research purpose for which it was designed. As described in Section 3.2, to build a mechanical breast model, one need to provide the breast geometry in a reference configuration, the constitutive models of tissues comprising the breast volume and the boundary conditions. The definition of all variables positing the breast volume and the boundary conditions. The definition of all variables has an significant impact on model accuracy.

Biomechanical modelling of breast tissues is widely investigated for various medical applications such as surgical procedure training, pre-operative planning, diagnosis and clinical actions such as surgery, image guided surgery, image registration, and material properties. For the last 20 years, several research groups have presented their breast models based on finite elements theory. The complexity and relevance to breast anatomy of each model 3.3). On the other hand, several researchers have presented their breast models based on finite elements theory. The complexity and relevance to breast anatomy of each model

3.5 Breast biomechanical model: overview

The biggest challenge here is that the magnitude of the stiffness constants is completely unknown beforehand. The contact force at each node have to be large enough to push the contact surface back to the target surface and eliminate unwanted penetration gap. In the same time, if the contact force is too large, it pushes the contact surface far away from the pinball region causing errors and solution instabilities.

where d represents the penetration or gap amount and k_c is the normal contact stiffness of opening contact stiffness constants respectively. The tangential contact stiffness works in the same way enforcing the responding frictional force. Some finite amount of penetration, $d > 0$, is required mathematically to maintain equilibrium. However, physical contacting bodies do not penetrate ($d = 0$).

$$p^c k = c f$$

Force is computed using the following expression:

The penalty method uses a spring-like relationship to introduce a force for all nodes pairs (contact-target) that are deformed to be in closed contact (Figure 3.4). The contact

The numerical calculations but have no physical meaning.

Properties are defined to manage contact behavior as: normal stiffness factor and contact opening factor. The latter constants play an important role in simulating contacts between objects.

using penalty method. Then one is using penalty constraint formulation, additional contact

Pure Penalty method
In this work, mathematical expression of contact compatibility conditions is formulated

Dear Doctor, I am a 25-year-old male who has been experiencing persistent pain in my lower back and right leg for the past month. The pain is particularly severe at night and when I sit for extended periods. I have tried over-the-counter pain relievers without relief. I would appreciate your advice on what steps to take next.

measures are computed for each mesh node of the discretized surface.

elements are named contact and target elements respectively. They have no material properties apart from friction coefficient μ . The stress-strain as well as the gap or penetration

ear or quadratic elements consistent with the underlying 3D element mesh (Figure 3.7). The

For the finite element calculations, contact and target surfaces have to be discretized in 2D lin-

Finite element mesh

are time-consuming and in very uncomfortable in a clinical framework. Even though the estimated geometries are accurate enough, these methods configuration by applying a hydrostatic distributed load on the breast surface in prone configuration by imaging the breast immersed in water. Following the same physical assumptions, Kuhlmann et al. (2013) proposed to estimate the stress-free the breast stress-free configuration by imagining the breast immersed in water. Following the same physical assumptions, Kuhlmann et al. (2013) proposed to estimate the stress-free assuming that breast density is equal to water density, Rajagopal et al. (2008) compute

90

Breast neutral buoyancy configuration

state and can be used only with small deformations or highly constrained models. et al. (2014) the inverse gravity method gives a poor approximation of the breast reference consideration of pre-stresses of breast tissues in prone configuration. According to Ebden the stress-free geometry. In their work, the authors just reversed the gravity effects without (Palomar et al., 2008; Sturgeon et al., 2016) used the inverse gravity method to estimate

95

Inverse gravity

frame-work, as a multi-loading simulation the latter assumption highly penalizes simulation are negligible when compared to the compression induced stress. However, for a different is justified only for a breast compression simulation, as the gravity induced pre-stresses is considered only for a prone body position, neglecting tissues pre-stresses. This assumption configuration in prone body position, neglecting tissues pre-stresses. This assumption (2006) and Sturgeon et al. (2016) have estimated breast compression starting from breast only in a up-right or prone body position. Therefore, Han et al. (2012), Ruitter et al. considering existing image modalities, in a clinical framework woman breast is compressed

970

results.

Prone breast configuration

estimate the breast reference configuration. The bibliography presents four different strategies allowing to them in clinical conditions. The generally unknown and it is extremely difficult to measure The initial pre-stresses are generally unknown and it is extremely difficult to measure in a stress-free configuration, without being deformed by any force, including gravity. in a stress-free configuration, the reference configuration is chosen to be the breast geometry to in-vivo conditions, and therefore initial pre-stresses are included. Generally, for breast deformation simulation, the reference configuration is chosen to be the breast geometry to compute the breast geometry. Aged data represents deformed breast soft tissues due to Martinez-Martinez et al. (2017) or CT images Palomar et al. (2008); Sturgeon et al. (2016); images Carter (2009b); Kellner et al. (2007); Connely et al. (2015); Ebden et al. (2016); A large number of existing patient-specific models are using volume metric data from MR

990

3.5.1 Breast reference configuration

CHAPTER 3. BACKGROUND AND STATE OF THE ART

Background information about breast geometry if the patient is in a supine position and how acquisition and processing of images can significantly shorten post-processing for analysis.

11

Neo-Hookean material models are considered, the range of the adipose and glandular shear observed between the linear elastic and hyperelastic models. If only in-vivo studies with 1040

An important difference in estimated values of elastic moduli of breast soft tissues is 1041

elastic properties of the glandular tissues can change by about 30%. 1042

et al. (2003) showed that during the mechanical cycle, due to the hormonal changes, the 1043

individual variability, with the shear modulus ranging between 0.22 – 43.6 kPa. Lorenzen 1044

For example, Han et al. (2012) though using the same FE method, found significantly inter- 1045

set-up but also by the participant's physical condition, age or period of the experimental 1046

271.8 kPa. Such big variation may be explained by the differences in the used experimental 1047

and glandular tissues. The breast tissues elastic parameters range between 0.1 kPa and 1048

Later, several research groups (Table 3.2) have studied the elastic modulus of adipose 1049

from 5% to 20% pre-compression. 1050

of invasive carcinoma is from 5 to 25 times larger than the one of normal adipose tissue 1051

Krouskop et al. (1998) found that depending on the pre-compression level, Young's modulus 1052

ones of the normal breast tissues, in a study of 142 samples, following to 4 type of tissues, 1053

breast is developing benign or malignant disorders, their mechanical properties differ from the 1054

anatomical properties estimation of breast tissues were done in diagnostic purposes. Then the 1055

degree subsatinal changes during woman lifetime (section 7). The first studies on mech- 1056

multiple studies have shown that breast composition and so its mechanical behavior un- 1057

Glandular and adipose tissues biomechanical properties

Neo-Hookean model proposed by Rajagopal et al. (2008) gives the best estimates. 1058

most popular models in a multi-loading gravity simulation according to the authors, the 1059

2006; Carter et al., 2012; Martinez-Martinez et al., 2017). Edler et al. (2014) compared the 1060

Han et al., 2014; Garcia et al., 2017), Mooney-Rivlin (Samanie et al., 2007; Tammer et al., 1061

elastic (Carter, 2009b; Rajagopal et al., 2010; Sturgeon et al., 2016; Eiben et al., 2016a; 1062

response to a external force: exponential elastic (Azaar et al., 2002), Neo-Hookean hyper- 1063

For the last decades several constitutive models were used to model the breast tissues 1064

equal to 9810 kg/m³. 1065

tissues are predominantly composed of water; therefore, the density is considered to be 1066

the best estimates are obtained with high Poisson ratio ($\nu = 0.495, 0.499$). The soft breast 1067

linear constitutive models was studied by Tammer et al. (2006) according to the authors, 1068

a Poisson ratio ranging between $\nu = 0.45 - 0.5$. The influence of the Poisson ratio within 1069

blood flows, thus, soft tissues are frequently modeled as quasi-incompressible materials with 1070

Under large compression and body position change the breast volume varies due to the 1071

scales. 1072

tissues viscosity can be neglected when the mechanical load is applied within short time 1073

anisotropic, and viscous materials. However, according to Welleman et al. (1999) the breast 1074

mechanical properties. The breast soft tissues are known to be incompressible, nonlinear, 1075

global breast mechanics are governed by breast tissue compositions and their individual 1076

3.5.2 Constitutive models

Previously listed researchers clearly showed the variability of elastic modulus of the same tissue between and within individuals. Edler et al. (2014) made a larger analysis including were given by the Neo-Hookean model with the initial shear modulus equal to $0.2 kPa$.
 the subject is re-positioned from the supine to the prone positions. The best estimates the Mooney-Rivlin models underestimates the tissues deformation by at least 75% when 1045 loading gravity simulation were thus performed on 3 subjects. According to the authors parameters Mooney-Rivlin potential function for various material properties. The multi Carter (2009b) compared one parameter Neo-Hookean potential function with five modulus is significantly lower than $50 kPa$.

Table 3.2: Material properties for adipose and glandular tissues.

Author	Method	Material	Ex-vivo estimation			In-vivo estimation												
			Adipose kPa	Glandular kPa	$E = 19 \pm 7$	$E = 20 \pm 6$	$E = 6.6$	$E = 33$	Wellman et al. (1999)	Wellman et al. (1999)	Van Houten et al. (2003)	Simkus et al. (2005)	Bajagopal et al. (2008)	Carter (2009a)	Han et al. (2012)	Gamagae et al. (2012)	Griesenauer et al. (2017)	
Krouskop et al. (1998)	Indentation	Linear elastic	$E = 20 \pm 6$	$E = 57 \pm 19$	$E = 20 \pm 6$	$E = 6.6$	$E = 33$	$E = 33 \pm 11$	$E = 3.24 \pm 0.61$	$E = 3.25 \pm 0.91$	$E = 17.4$	$E = 271.8$	$\mu = 0.16$	$\mu = 0.4$	$E = 0.22$ - 43.64	$\mu = 0.1$	$E = 0.25$	$E = 2$
Krouskop et al. (1998)	Indentation	Linear elastic	$E = 19 \pm 7$	$E = 33 \pm 11$	$E = 19 \pm 7$	$E = 6.6$	$E = 33$	$E = 33 \pm 11$	$E = 3.24 \pm 0.61$	$E = 3.25 \pm 0.91$	$E = 17.4$	$E = 271.8$	$\mu = 0.16$	$\mu = 0.4$	$E = 0.22$ - 43.64	$\mu = 0.1$	$E = 0.25$	$E = 2$
Samani and Plewes (2004)	Indentation	Linear elastic	$E = 3.25 \pm 0.91$	$E = 3.24 \pm 0.61$	$E = 3.25 \pm 0.91$	$E = 3.24 \pm 0.61$	$E = 3.25 \pm 0.91$	$E = 17.4$	$E = 271.8$	$\mu = 0.16$	$\mu = 0.4$	$E = 0.22$ - 43.64	$\mu = 0.1$	$E = 0.25$	$E = 2$			
Van Houten et al. (2003)	MRE	Linear elastic	$E = 17 - 26$	$E = 26 - 30$	$E = 17 - 26$	$E = 26 - 30$	$E = 17 - 26$	$E = 26 - 30$	$E = 17 - 26$	$E = 26 - 30$	$E = 17.4$	$E = 271.8$	$\mu = 0.16$	$\mu = 0.4$	$E = 0.22$ - 43.64	$\mu = 0.1$	$E = 0.25$	$E = 2$
Simkus et al. (2005)	MRE	Visco-elastic	$\mu = 2.9 \pm 0.3$	$\mu = 2.9 \pm 0.3$	$E = 17.4$	$E = 271.8$	$\mu = 0.16$	$\mu = 0.4$	$E = 0.22$ - 43.64	$\mu = 0.1$	$E = 0.25$	$E = 2$						
Bajagopal et al. (2008)	MRI-FEM	Neo-Hookean	$\mu = 0.16$	$\mu = 0.26$	$\mu = 0.16$	$\mu = 0.26$	$\mu = 0.16$	$\mu = 0.26$	$\mu = 0.16$	$\mu = 0.26$	$E = 1$	$E = 0.22$ - 43.64	$\mu = 0.1$	$\mu = 0.1$	$E = 0.25$	$E = 2$	$E = 0.25$	$E = 2$
Carter (2009a)	MRI-FEM	Neo-Hookean	$\mu = 0.25$	$\mu = 0.4$	$\mu = 0.25$	$\mu = 0.4$	$\mu = 0.25$	$\mu = 0.4$	$\mu = 0.25$	$\mu = 0.4$	$E = 1$	$E = 0.22$ - 43.64	$\mu = 0.1$	$\mu = 0.1$	$E = 0.25$	$E = 2$	$E = 0.25$	$E = 2$
Han et al. (2012)	MRI-FEM	Neo-Hookean	$E = 1$	$E = 1$	$E = 1$	$E = 1$	$\mu = 0.1$	$\mu = 0.1$	$E = 0.25$	$E = 2$	$E = 0.25$	$E = 2$						
Gamagae et al. (2012)	MRI-FEM	Neo-Hookean	$\mu = 0.1$	$\mu = 0.1$	$\mu = 0.1$	$\mu = 0.1$	$\mu = 0.1$	$\mu = 0.1$	$E = 0.25$	$E = 2$	$E = 0.25$	$E = 2$						
Griesenauer et al. (2017)	MR-FEM	Neo-Hookean	$E = 0.25$	$E = 2$	$E = 0.25$	$E = 2$	$E = 0.25$	$E = 2$	$E = 0.25$	$E = 2$	$E = 0.25$	$E = 2$	$E = 0.25$	$E = 2$	$E = 0.25$	$E = 2$	$E = 0.25$	$E = 2$

with respect to the input parameters.

To our knowledge, where are no experimental data describing the mechanical properties of breast superficial fascia. An approximation of the elastic modulus of Cooper's ligaments is given by Gelen and Dillimoney (2007) by extrapolating from known ligamentous structures

The suturing technique breast fascias and the superficial ligament form the breast support matrix. These structures are well described for surgical purposes (thickness, location etc), however little is known about their mechanical properties. The first biomechanical breast model taking into account the effect of Cooper's ligaments was proposed by Aza et al. (2002) and took up later by Patilmanathan et al. (2008) and Han et al. (2012). The authors designed a new material model for fatty tissues including the anisotropic behavior of breast ligaments. Later, Georgii et al. (2016) come up with a spring-mass generic model for the breast support matrix. According to the authors, including the ligaments into the finite elements breast model have increased the robustness of the prone-supine simulation with respect to the input parameters.

Fascias and ligaments biomechanical properties

The estimation of the breast skin elasticity by the means of finite elements using Neo-Hookean potential function has resulted in softer materials model. Carter (2009a) found a initial shear modulus equal to $16kPa$, whereas Han et al. (2014) found that for the five studied subjects the skin shear modulus ranged between $2.47kPa$ and $5.78kPa$.

Other researches on skin elasticity are available, but they are not specific to the breast skin. Hendrikx et al. (2006) estimated in-vivo skin properties by suction testing. The skin was considered as a homogeneous, isotropic, incompressible, hyperelastic material. The study was performed on 14 subjects and the obtained average of elastic modulus for skin was 58.4 kPa.

Sutradhar and Miller (2013) published a complete study of breast skin estimating its elasticity for 16 different breast regions. The study was done on 23 female volunteers aging from 29 to 75 years. The authors found that the skin elasticity modulus ranged between 15 – 480 kPa with an average of 334 ± 88 kPa. The elastic modulus in the lateral region (mean 370 kPa) has the highest value followed by the superior region (mean 355 kPa). The inferior region (mean 331 kPa) follows next, with the medial region having the lowest value (mean 316 kPa). However, no significant variation of elastic modulus in radial direction was found.

Several studies show the importance of skin in biomechanical breast modeling. According to Carter (2009b), a model which includes the skin estimate better the tissue deformation under gravity loading.

skin biomechanical properties

Muscle biomechanical properties.

all material models proposed in the literature. According to authors, many of them are too stiff permitting not enough deformation within the gravity loading. The most reliable identified values is the ones given by Rajagopal et al. (2008) (Table 3.2). In addition

During the last decades, several breast biomechanical models were proposed. However, only a small part of them (Carter, 2009b; Gamagie et al., 2012; Han et al., 2014) were evaluated with respect to the real tissues deformations. As we intend to build-up a subject specific breast biomechanical model capable of estimating multi-loading gravity deformations our assumption will rely only on already evaluated model within a same framework.

Today's outstanding breast biomechanical models are represented by the next three models: Eiblén et al. (2016c), Han et al. (2014), Gamagie et al. (2012). Gamagie et al. (2012) proposed a finite elements model capable to estimate the supine breast configuration from the prone one. To assess the quality of fit, the root-mean-squared error (RMSE) form the point to surface distance was computed. Conform to the authors, the breast supine geometry was estimated within an RMSE of 5 mm (maximal distance of 9.3 mm). In the same time, Han et al. (2014) developed a breast biomechanical model for image registration. The estimates were computed for five subjects, and the accuracy was assessed by comparing the Euclidean Distance (ED) between anatomical landmarks. The mean ED range between

3.5.4 Conclusion

Direkt conditions are usually used to constrain the sternum/axilla ends and the posterior surface of the breast or the thoracic cage if the muscular tissues are considered (Griesenauer et al., 2017; Rajagopal et al., 2008; Pathmanathan et al., 2008; Gamaagé et al., 2012; Griesenauer et al., 2017). As reported by Carter (2009b) the zero-displacement boundary condition in a multi-gravity loading framework result in a over-constrained model and sliding conditions on the mesh nodes corresponding to the chest wall have to be considered. Later, several teams using biomechanical breast models for multi-modality image registration or surgical planning showed what it included the sliding boundary conditions (Georgii et al., 2016; Han et al., 2014) improve the registration accuracy. However those studies were the biomechanical model is designed for breast compression, the issues sliding over the chest wall is neglected and fixed boundary conditions are usually assumed (Sturgeon et al., 2016; Martínez-Martínez et al., 2017).

3.5.3 Boundary conditions

The fibrous tissues obtain their elasticity from elastic fibers and their structural support from collagen fibers. As reported by Higgió et al. (2000), the superficial fascia is made up of both collagen and elastic fibers. In contrast, the Cooper's ligaments appear to be composed almost of collagen fibers. The mechanical properties of a single collagen fiber from a rat tail were studied by Wengger et al. (2007) according to authors their elastic modulus ranges between 5GPa and 11GPa. Other studies on biomechanical characterization of human body superficial fascia are available in literature. The most frequently studied is on the plantar fascia and foot ligaments with a Young's modulus ranging between 0MPa and 700MPa (Chenig et al., 2004; Kongsgaard et al., 2011).

Perd-erà que en la seva ciutat, la personalitat d'una ciutat en polifòrmica
de transició ha de ser la mateixa, dividida per la seva
elaboració en model històric que posa en conjunt les
fàbriques i els edificis que fan part de la seva
modelles de soldats (com es podria fer en el cas general),
i amb unes suposicions com les fàbrics del Llobregat, que
modifica els models (com es podria fer en el cas general) i
el seu poble els estàtuts per solucionar això.

11.5 mm and 39.2 mm (maximal ED range between 20.3 mm and 61.7 mm). Finally, Eiben et al. (2016c) proposed a new model to estimate the up-standing breast configuration from the prone one. The model was evaluated on 3 subjects. The supine configuration was then computed from the prone one and the quality of fit was measured in terms of the mean Eulerian Distance between manually selected internal landmarks. Thus, the supine breast configuration was estimated within a mean distance ranging between 12.2 mm and 19.8 mm. The model evaluation for the up-standing configuration was not presented.

Authors	Application	FE mesh	Material models	Boundary conditions	Stress-free config.
Azar et al. (2002)	Computer assisted breast surgery	8-Node hexahedrons (trilinear isotropic elements)	Skin-elastic linear, adipose,glandular-hyperelastic polynomial	Sliding between breast - thorax and breast-paddle	Prone breast geometry
Rajagopal et al. (2007)	Breast compression	8-Node hexahedrons (tricubic Hermite elements)	Homogeneous , Neo-Hookean model	Zero-displacement BC	Buoyant breast in water
Pathmanathan et al. (2008)	Image registration	8-Node hexahedrons (trilinear elements)	Homogeneous polynomial hyperelastic; Skin exponential hyperelastic	Zero-displacement on muscle; Compression with imposed displacement	Inverse FE algorithm
Han et al. (2014)	Image registration	4-Node tetrahedrons	Muscle, glandular, fatty, skin - Neo-Hookean model	Sliding on pectoral muscle	Inverse gravity
Gamage et al. (2012)	Computer assisted breast surgery	8-Node hexahedrons (tricubic Hermite elements)	Homogeneous+ Neo-Hookean incompressible muscle-Neo-Hookean model	Zero-displacement BC on rib cage surface, Sternum, axilla ends, shoulder	PC iterative algorithm
Patete et al. (2013)	Computer assisted breast surgery	4-Node tetrahedrons (trilinear isotropic elements)	Adipose , glandular, skin	Zero-displacement BC on the chest wall	PC iterative algorithm
Kuhlmann et al. (2013)	image registration	4-Node tetrahedrons	Adipose, glandular- linear gel-like (Eulerian formulation); Skin - hyperelastic material (Lagrangian formulation)	Zero-displacement chest wall	PC iterative algorithm
Georgii et al. (2016)	Surgery simulation	8-Node hexahedrons, 2-node 3D spars	homogeneous elastic material, Cooper's ligaments-generic mass-spring model	sliding BC (breast on the pectoral muscle)	NA
Eiben et al. (2016c)	Surgery outcome prediction	4-Node tetrahedrons	Fatty , glandular- Neo-Hookean model; skin-exponential hyperelastic	Zero-displacement BC	Inverse FE algorithm
(Garcia et al., 2017)	3D breast lesion localization	4-Node tetrahedrons	adipose, glandular - Neo-Hookean models	zero-displacement BC	Prone breast configuration